The Effect of Average Soft Segment Length on Morphology and Properties of a Series of Polyurethane Elastomers. I. Characterization of the Series

DARREN J. MARTIN,[1,*] GORDON F. MEIJS,[2] GORDON M. RENWICK,[3] SIMON J. McCARTHY,[2] and PATHIRAJA A. GUNATILLAKE[2]

[1]Graduate School of Biomedical Engineering, University of New South Wales, Sydney, NSW 2052, Australia; [2]CSIRO Division of Chemicals and Polymers, Private Bag 10, Rosebank MDC, VIC 3169, Australia; and [3]Department of Materials Science, University of Technology, Sydney, Broadway, NSW 2007, Australia

SYNOPSIS

A series of eight thermoplastic polyurethane elastomers were synthesized from 4,4'-methylene diphenyl diisocyanate (MDI) and 1,4-butanediol (BDO) chain extender, with poly(hexamethylene oxide) (PHMO) macrodiol soft segments. The soft segment molecular weights employed ranged from 433 g/mol to 1180 g/mol. All materials contained 60% (w/w) of the soft segment macrodiol. Differential scanning calorimetry (DSC), dynamic mechanical thermal analysis (DMTA), wide angle x-ray diffraction (WAXD), and small angle x-ray scattering (SAXS) techniques were employed to characterize morphology. Tensile and Shore hardness tests were also performed. Materials were tested in the annealed state. It was found that an increase in segment length was accompanied by an increase in the degree of microphase separation, average interdomain spacing, hard domain order, hardness, stiffness, and opacity. DSC experiments showed the existence of several hard segment melting regions that were postulated to result from the disordering or melting of various hard segment length populations. For the system and composition ratio employed, it was found that optimum tensile properties (UTS and breaking strain) were achieved when a PHMO molecular weight of between 650 and 850 was utilized. © 1996 John Wiley & Sons, Inc.

INTRODUCTION

Polyurethane elastomers are linear segmented copolymers with an $[HS]_n$-type structure, where H and S represent hard and soft segments, respectively, and where H and S both involve a distribution of sequence lengths. In the solid state, unique elastomeric properties are observed due to microdomain formation. The so-called hard domains provide both physical crosslink sites and filler-like reinforcement to the soft segment matrix. At higher temperatures, a homogeneous melt can be formed allowing the material to be thermally processed.

An understanding of morphology is critical to the rational design of improved polyurethanes. Morphological factors such as degree of hard/soft phase separation, crystallinity, and domain size/shape influence properties such as hardness, stiffness, tensile strength, and clarity.

The morphology and properties of thermoplastic polyurethane elastomers are greatly influenced by the compatibility of starting compounds,[1-4] the ratio of hard and soft block components,[2,5-13] the average block lengths employed (including molecular weight distribution),[13-21] the thermal history of the material,[11,19,22,33] and the mechanical history experienced by the material.[34-37]

This article reports the effects of changing the length of the soft and hard segments in a series of fixed soft segment concentration (wt % soft segment = 60%) polymers.

In this study it has been advantageous to have a large series of polyurethanes made from macrodiols with relatively small molecular weight differences. Previous studies of this kind[14-17,19] have utilized fewer polymers with soft segments having larger

* To whom correspondence should be addressed.

Journal of Applied Polymer Science, Vol. 62, 1377–1386 (1996)
 CCC 0021-8995/96/091377-10

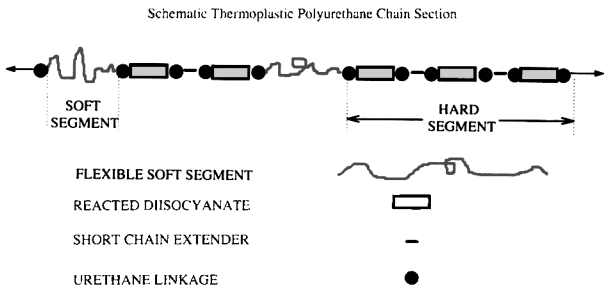

molecular weight differences (e.g., ca 1000, 2000, and 3000) and have not involved PHMO soft segment. The range of soft segment molecular weights chosen for this series envelopes the "useful" range of possibilities for this particular system and composition ratio.

EXPERIMENTAL SECTION

Materials and Synthesis

All eight polyurethanes included hard segments comprised of MDI and BDO, and a macrodiol weight percent of 60%. A molar isocyanate excess of 3% was employed. The poly(hexamethylene oxide) macrodiols employed had the general structure:

$$HO-[(CH_2)_6-O-]_n-H$$

These PHMO macrodiols were synthesized by condensation polymerization of 1,6-hexanediol.[38] As the condensation polymerization proceeded, samples of polyol were extracted from the reaction vessel at predetermined time intervals. The hydroxyl numbers of all macrodiols were determined by a standard procedure (ASTM D2849-method C).[39] The MDI and BDO were distilled and degassed, respectively, and all polyols were dried thoroughly under a vacuum of better than 0.1 Torr at 105°C for at least 12 h prior to synthesis.

Synthesis of the polyurethanes involved one-step bulk polymerization. Dried macrodiol was accurately weighed into a clean, dry polypropylene beaker, and kept dry at 105°C in an oven under a vacuum of 0.1 Torr prior to polymerization. Degassed BDO was weighed into a prewet, tared polypropylene syringe and added to the dried macrodiol in the reaction beaker. Freshly distilled MDI was weighed into a wet tared polypropylene beaker and immediately added to the reaction beaker, which was then stirred continuously with a spatula for 1 min to ensure uniform mixing of all ingredients. The contents of the reaction beaker were poured onto a Fibreglas-reinforced Teflon sheet, covered with a second sheet and pressed by hand to a thickness of less than 5 mm. The as-poured material was then placed in an oven to cure at 120°C for 4 h under a steady flow of dry nitrogen.

The polymers were compression molded into either 0.5 mm thick sheets (for SAXS and DSC samples) or 1.3 mm thick plaques (for other tests) at a temperature of 200°C using a water-cooled hydraulic press. The cooling procedure was kept uniform for all materials by carefully controlling the water flow rate.

Annealing was carried out on predried sheets/plaques (0.1 Torr at 40°C overnight) under a dry nitrogen purge at 135°C for 10 h. The sheets were allowed to cool to room temperature slowly in the oven. All morphological tests were carried out on annealed samples. Tensile, hardness, and GPC measurements were carried out on material in the as-molded condition only.

Instrumentation and Methods

Molecular weight analysis of the as-molded materials was carried out on a Spectra Physics GPC system using *N,N*-dimethylformamide containing 0.05*M* LiBr as the mobile phase. Columns of pore size 10^2, 10^3, and 10^5 Å were employed, and the system was calibrated against six polystyrene standards.

DSC measurements for the polyurethane samples were performed on a TA Instruments DSC2920 with a 10°C/min heating rate. DSC samples were dried (0.1 Torr at 40°C overnight) prior to testing, and a sample weight of about 10 mg was used. The pure PHMO macrodiols were tested on a Mettler DSC 30 using the same run conditions.

Dynamic mechanical testing was carried out on a Polymer Laboratories DMTA equipped with tensile head and reducing force option, with a heating rate of 2°C/min and frequency setting of 2 Hz.

Wide-angle x-ray diffraction work was carried out on a Siemens D5000 diffractometer using CuK_α radiation.

Small-angle x-ray scattering was performed on the SAXS facility at the Research School of Chemistry, the Australian National University (ANU), Canberra. This machine has been briefly described elsewhere.[40] The radiation used was CuK_α. A preliminary set of measurements was made on 1.3 mm thick samples. Strong scattering functions were recorded, but the multiple scattering present was unacceptable and so samples 0.4 mm thick were prepared and utilized. The data were corrected for detector sensitivity and electronic background.

Table I PHMO Macrodiol Molecular Weights and Thermal Transitions

PHMO Molecular Weight ($g \cdot mol^{-1}$)	Melting Temperature (°C)	Enthalpy of Fusion ($J \cdot g^{-1}$)
433	30.0	102.8
476	36.8	114.6
650	39.1	116.9
708	41.2	122.2
793	42.5	126.3
851	44.5	128.2
998	47.0	129.8
1180	47.2	128.4

Transmission and flux measurements were carried out before and after each test. The sample-to-detector distance was 890 mm. No desmearing of the data was performed. All data were corrected using a water-scattering function to an absolute scattering intensity scale (units of cm^{-1}). Data were processed using the BLISS program at the Research School of Chemistry, ANU, and the ANU-ORNL data analysis software.

Tensile testing was carried out on five replicates of each material with an Instron model 4032 universal testing machine. Smaller-than-standard tensile dumbbell samples were punched from the moulded sheet stock. The smaller samples (t = 1.3 mm, w = 4.3 mm, l = 30 mm) were required to allow for large elongation behavior and to enable a comparison with previous tensile results,[4,41-43] which employed the same sized dumbbell samples. A 1 kN load cell was used and the crosshead speed was 500 mm/min. Gauge lengths of 20 mm were used, and pneumatic grips were required to hold the test specimens. Shore hardness values were measured at 22°C with calibrated A and D scale indentors by stacking five 1.3 mm thick moldings together on a flat surface.

RESULTS AND DISCUSSION

Characterisation of Pure Macrodiols

Table I shows the molecular weight, melting temperature, and enthalpy of fusion values for the pure macrodiols. In a previous study,[4] the glass transition temperature for rapidly quenched pure PHMO of 1000 molecular weight was determined to be −35°C. In the same study, wide angle x-ray diffraction was carried out on the waxy PHMO compound, and very strong diffraction peaks were found with lattice spacings of 4.52 Å and 3.69 Å.

As would be expected, the macrodiols in Table I show an increase in melting temperature and enthalpy of fusion accompanying higher molecular weights. The relatively high enthalpy of fusion values indicate a high degree of crystallinity.

Characterization of Polyurethane Series

Nomenclature Employed

The nomenclature used for this series is of the form H####, where the number following H represents the molecular weight of PHMO macrodiol employed in the polymer.

Polyurethane Formulations

When synthesizing this series two parameters were held constant. A constant wt % fraction of 60% soft segment, and a 3% molar excess of isocyanate groups with respect to hydroxyl groups. This means that the materials containing shorter soft segments must include a larger number of shorter hard segments with more isocyanate end groups to satisfy these above requirements. That is, as the average soft segment length is decreased, the average hard segment lengths are also decreased and hard segments become more rich in MDI content (less BDO). This change in hard segment lengths and compositions is more easily seen in Table II and Figures 1 and 2. As the soft segment length is increased, the resultant copolymer changes from what is essentially an alternating MDI-PHMO structure (e.g., H433) containing very few "real hard segments" (i.e., those including BDO), through to a copolymer including a larger number of hard segments containing an average of approximately 2 MDI units and 1 BDO unit (e.g., H708), and finally, in the copolymer with the longest soft segments (H1180) we would expect to find large numbers of both MDI-BDO-MDI and MDI-BDO-MDI-BDO-MDI hard segment se-

Table II Molar Ratio of Ingredients for PU Series

Material	PHMO (mol)	MDI (mol)	BDO (mol)
H433	1	1.12	0.09
H476	1	1.21	0.17
H650	1	1.55	0.51
H708	1	1.67	0.62
H793	1	1.84	0.78
H851	1	1.96	0.89
H998	1	2.25	1.18
H1180	1	2.59	1.52

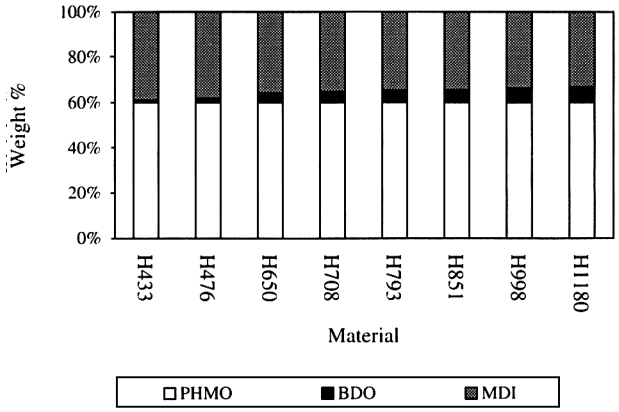

Figure 1 Composition by weight of the series.

quences. In all cases there will be a broader distribution of sequence lengths than shown in Figure 2, and in all cases there will be at least a small number of single MDI hard segments present.[44,45]

Differential Scanning Calorimetry

Figure 3 shows the DSC thermograms for the polyurethane series after annealing at 135°C for 10 h. Peak temperatures and enthalpy values are listed in Table III. An increase in soft segment length causes a decrease in the soft microphase T_g (indicated by arrows) and also a decrease in the associated change in specific heat. These trends indicate an increase in soft domain purity.

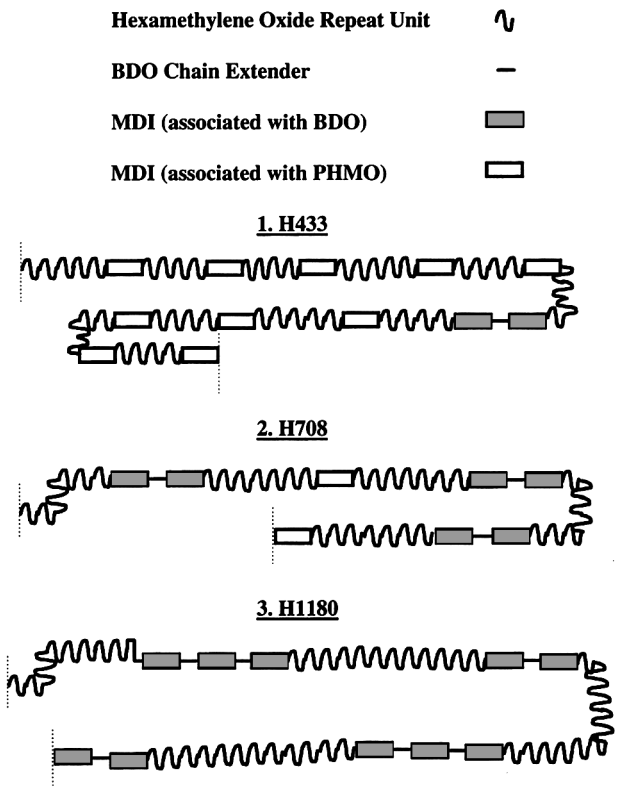

Figure 2 Schematic representation of H433, H708, and H1180 chain sections.

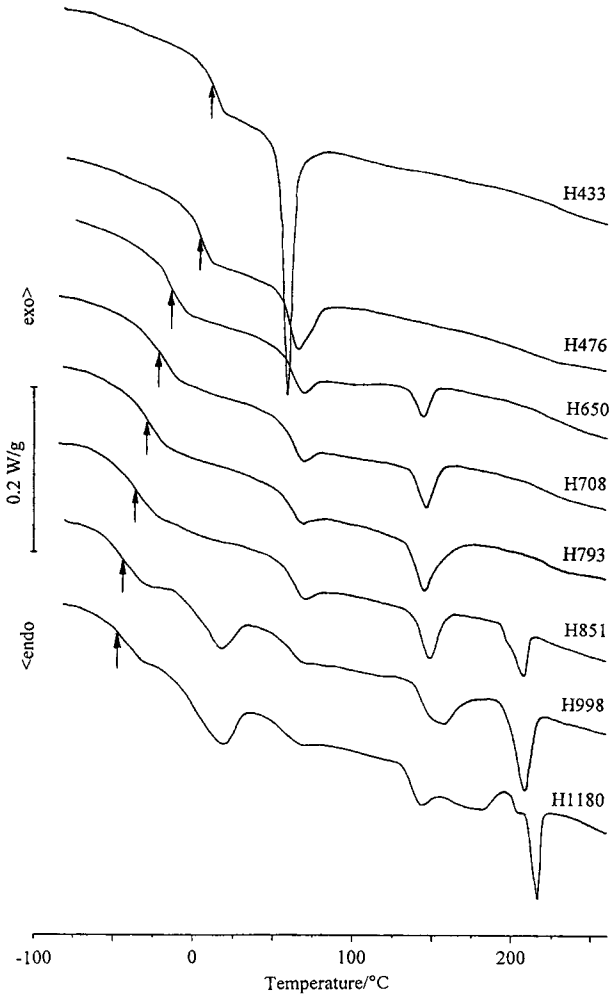

Figure 3 DSC thermograms for the series annealed at 135°C and tested at a heating rate of 10°C/min.

Thermograms for the H998 and H1180 samples include broad endotherms, which follow the soft segment T_g. Similar endotherms were encountered in a previous study for poly(octamethylene oxide) (POMO) and poly(decamethylene oxide) (PDMO)-based polyurethanes and were attributed to soft segment "paracrystallinity."

The large, sharp endotherm observed in the H433 thermogram is believed to arise from either the melting of a fringed micelle microstructure or from the disruption of non-ideally-packed single MDI-derived urethane linkages. This type of structure is afforded by the materials very short block lengths and more homogeneous urethane group distribution and, hence, hydrogen bonding capacity along the polymer chains. More evidence for this structure is shown in the SAXS results where no contrast in

Table III Summary of DSC Features for Series 2 Materials Annealed at 135°C

Material	Soft Phase T_g/°C	Soft Phase Disordering[d]/°C	Hard Phase T_g/°C	Intermediate Endotherm Melting/°C, (ΔH/Jg^{-1})	Hard Phase Melting/°C (1st, 2nd)	Hard Phase ΔH/Jg^{-1} (1st, 2nd)[a]
H433	14.2	*	*	58.8, (14.8)[b]	*	*
476	−5.0	*	*	64.6, (6.2)[b]	*	*
H650	−15.9	*	62.7	68.1, (0.9)[c]	143.1	6.3
H708	−19.2	*	62.2	67.2, (0.7)[c]	145.2	10.0
H793	−30.5	*	62.3	67.3, (0.5)[c]	144.7	16.0
H851	−34.0	*	63.2	68.8, (0.4)[c]	147.4, 206.3	11.3, 8.3
H998	−38.4	15.3	61.3	*	154.4, 207.0	13.8, 26.8
H1180	−40.5	15.6	61.2	*	142.2[br], 215.9	25.3[br], 12.8

[a] Enthalpy of fusion values for hard phase melting were calculated "per gram of hard segment" rather than per gram of polymer.

[b] These endotherms seen for the H433 and H476 polymer were ascribed to melting of a fringed micelle morphology where "whole chain" folding occurs rather than the "bundle crystallinity" common to the hard microphases in the other samples.

[c] Small endotherms due to enthalpy relaxation in the interface between hard and soft domains.

[d] Broad endotherms attributed to enthalpy relaxation of soft segments that have "partially ordered" at low temperatures during the DSC run.

* No transition observed.

[br] Very broad peak.

electron density was encountered. This signature is also present in the thermogram for H476 and to a decreasing extent through to H851. In H650 through to H851 it is believed the feature seen in this temperature region is actually a glass transition of the hard microphase and/or interfacial region, which is followed by a small endotherm associated with an enthalpy relaxation phenomena. In this process, a time-dependent densification of the initially amorphous hard domain fraction (including the hard–soft interface) occurs during aging at a temperature below the hard microphase T_g. This process is likely to involve the fraction of MDI units not associated with BDO, of which there are an increasing number as soft segment length is decreased (see Fig. 2). These single MDI units would be capable of a slow rearrangement because of their mobility and interurethane hydrogen bonding capacity. The hard domain glass transition is also observed in H998 and H1180; however, no enthalpy relaxation peaks are observed. Most of the MDI in these polymers would be associated with BDO in higher melting structures.

In H650 and above, a melting endotherm is present at around 145°C. In H650, H708, and H793 this is the only hard phase melting region, and the enthalpy of fusion values increase with segment length. It is believed that this endotherm, which is highly sensitive to annealing temperature (as shown in the SAXS-DSC annealing study in the following article) occurs due to the disordering of hard domain structures containing predominantly MDI-BDO-MDI hard segments (see molar ratios in Table II). We shall label this endotherm "T2."

A second higher endotherm appears at 207°C for H851 and H998, and is seen as a shoulder in H1180, which also has a sharp endotherm at 216°C. In these materials the T2 endotherm increases in enthalpy value but also broadens with further increase in segment length suggesting a more diverse range of hard segment "situations."

If we label the 207°C endotherms "T3" and the 216°C endotherm "T4," we can postulate that T3 and T4 represent melting of hard domain regions, which include predominantly MDI_3-BDO_2 and MDI_4-BDO_3 hard segments where these structures represent the longest extended hard segment sequences that are possible for the thermal conditions imposed and the degree of hard-soft compatibility in each particular material. Sequences longer than MDI_3-BDO_2 and/or MDI_4-BDO_3 must compete for space by somehow folding and reentering the hard domains and, thus, introducing defects in the structure. This phenomena could be an explanation for the broadening and increasing enthalpy observed for the T2 endotherms in the thermograms of H998 and H1180 that have the highest average segment lengths.

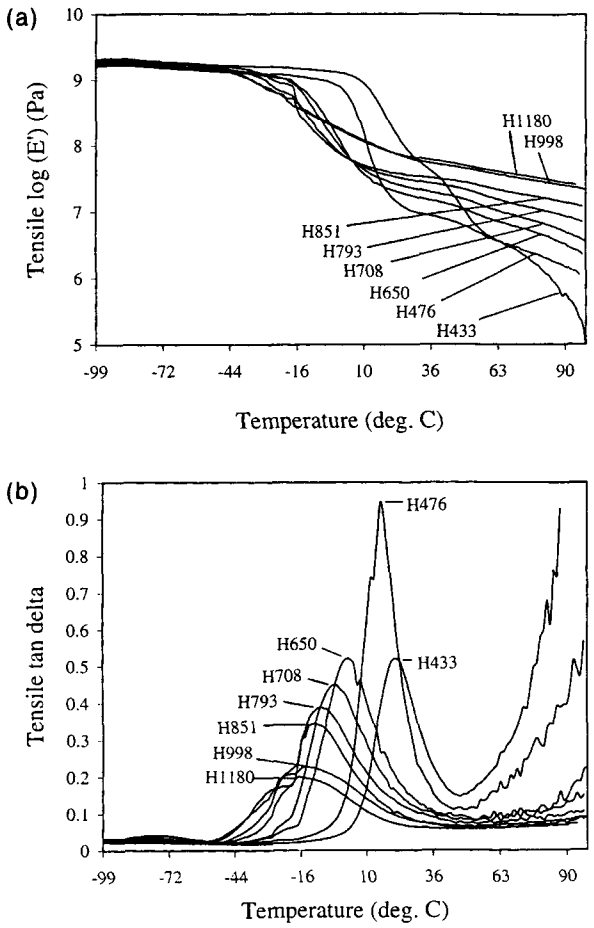

Figure 4 Dynamic mechanical behavior of the series tested at a heating rate of 2°C/min and at a frequency of 2 Hz. (a) Log storage modulus (E') vs. temperature. (b) Dissipation factor (tan δ) vs. temperature.

Dynamic Mechanical Behavior

Figure 4 illustrates the dynamic mechanical behavior of each material. The storage modulus (E') vs. temperature plot shows a drop in stiffness for each material accompanying the soft domain glass transition. At room temperature, apart from H433, which is above its T_g in this instance, an increase in soft segment length is accompanied by an increase in stiffness. This is due to a more developed microdomain structure in the longer block materials. The tan δ vs. temperature curves display loss peaks associated with the glass transition and damping capacity of the soft domains. The sharpness and height of the damping peaks give information about the degree of order and the freedom of motion of molecules in the soft domains. A flattening and broadening of the loss peaks occurs as longer soft segments are employed. This is also accompanied by a shift of the damping peaks to lower temperatures (as low as −17°C for H1180) indicating purer soft domains. The presence of crystallites is known to have an inhibiting effect on molecular motion in the amorphous regions; hence, a broadening and flattening effect on DMTA loss peaks.[46] This phenomena explains why the damping peak for H433 with its more crystalline structure is smaller than that of the more amorphous H476. Similarly, a more developed microdomain structure and purer soft domains in the polymers containing longer block lengths makes for an environment in which the motion of PHMO segments is more restricted.

Wide-Angle X-Ray Diffraction

Diffraction patterns for the annealed materials are shown in Figure 5. A diffraction peak at 16.4 degrees (d = 5.4 Å) was present in all samples (see Table IV). This peak is present for every material, regardless of the degree of phase separation or degree of crystallinity present.

This peak has also been reported in a previous study,[4] and in other similar studies by the authors[47] wherever a 3% molar excess of diisocyanate was employed. This peak position also does not match with literature values for MDI-BDO crystallinity.[12,22,29,48–52] It was thought that this peak may be due to a spacing between adjacent "single MDI"

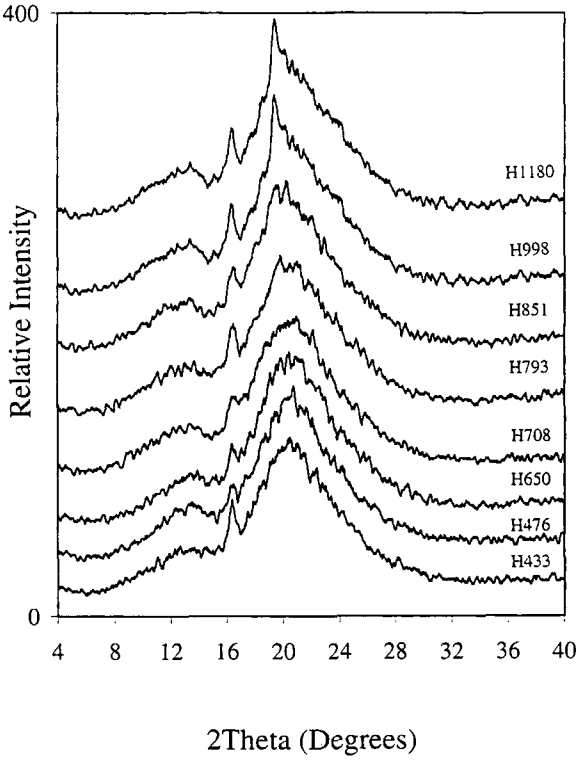

Figure 5 WAXD patterns for the series annealed at 135°C.

Table IV WAXD Peak Positions for Polyurethanes

Material	Diffraction Angles, 2θ	d-spacings (Å)
H433	16.38	5.41
H476	16.43	5.39
H650	16.38	5.41
H708	16.44	5.39
H793	16.43	5.39
H851	16.38, 19.58	5.39, 4.53[a]
H998	16.32, 19.54	5.43, 4.54[a]
H1180	16.32, 19.49	5.43, 4.55[a]

[a] d-spacing matches with literature MDI-BDO lattice spacings.

hard segments. To test this postulation a compound of MDI end capped with ethanol was synthesized and characterized by DSC and WAXD. This compound had a melting point of approximately 90°C. The diffraction pattern for this compound is shown in Figure 6. Importantly, a small diffraction peak matching with the 5.4 Å peak described above is observed, suggesting that it could be a result of single MDI hard segment stacking.

In Figure 5, the intensity of the central maxima is seen to grow and sharpen as segment length increases. H851, H998, and H1180 display a second peak at 4.54 Å due to hard domain crystallinity. This lattice spacing has been reported in the literature for the MDI-BDO unit cell.[12,29,48,51] Interestingly, the DSC thermograms for H851, H998, and H1180 (see Fig. 3) were the only ones that showed hard segment melting endotherms at temperatures above 200°C (T3 and T4 endotherms).

Small-Angle X-Ray Scattering

The SAXS camera used had a one-dimensional position sensitive detector and, therefore, the data collected required Lorentz correction. In this treatment the intensity is multiplied by Q^2, where Q is the scattering vector (defined by $Q = 4\pi/\lambda \sin\theta$, where θ is half the scattering angle). The intensity ($I(Q)$) of the small-angle scattering from a polyurethane depends on the difference in electron scattering length density ($\rho_h - \rho_s$) between the hard and soft microphases as given by:

$$I(Q) = K(\rho_h - \rho_s)^2 S(Q) \qquad (1)$$

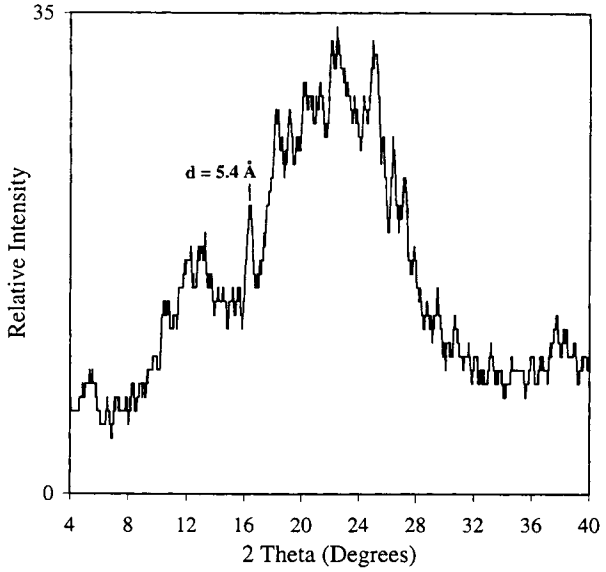

Figure 6 WAXD patterns for the ethanol end-capped MDI compound showing a small 5.4 Å diffraction peak.

where Q is the scattering vector, K is an instrument constant, and $S(Q)$ is the scattering function from the atomic particle distribution in the sample.

The intensity of the SAXS data also relates to the composition ratio of a material. The mean square electron density fluctuation, $\langle\rho^2\rangle$, is described by the relationship:

$$\langle\rho^2\rangle = \phi_h\phi_s(\rho_h - \rho_s)^2 \qquad (2)$$

where ϕh and ϕs are the respective volume fractions of hard and soft segments, which in turn, have elec-

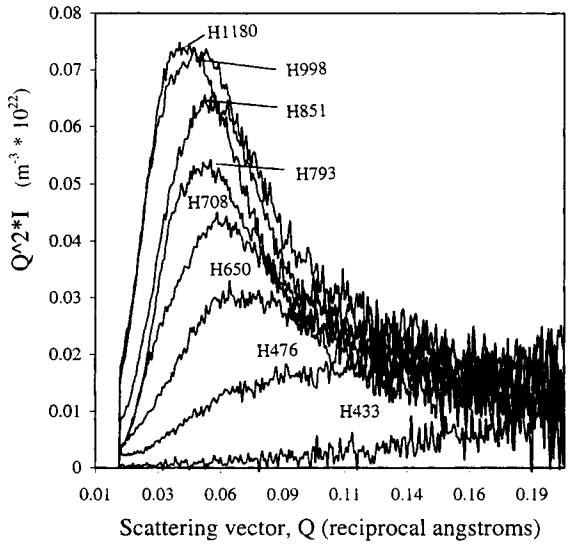

Figure 7 Lorentz-corrected SAXS curves for the series annealed at 135°C.

Table V SAXS Average Interdomain Spacing Values

Material	$Q_{max}/Å^{-1}$	$d_{Bragg}/Å$
H433	—	—
H476	0.0868	72
H650	0.0640	98
H708	0.0589	107
H793	0.0564	111
H851	0.0538	117
H998	0.0494	127
H1180	0.0437	144

tron densities ρ_h and ρ_s. Lorentz corrected SAXS data are shown in Figure 7.

The position of the scattering maxima, Q_{max}, can be used to estimate the average one-dimensional interdomain spacing, d_{Bragg}, by using Bragg's Law. The relationship between d_{Bragg} and Q_{max} for the camera used, is

$$d_{Bragg} = 2\pi/Q_{max} \quad (3)$$

where d_{Bragg} represents the average interdomain spacial periodicity or "long period."

Calculated long periods for the as-molded and annealed materials are shown in Table V.

The value obtained for this interdomain spacing is not a domain thickness value but rather an average spatial periodicity as presented in the very simplistic diagram below.

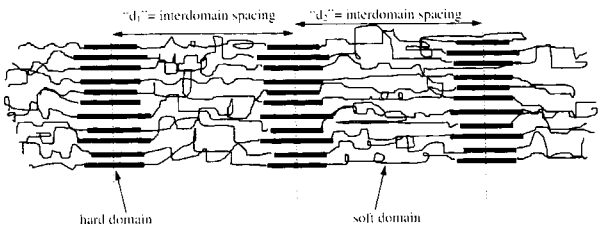

Longer segment lengths are accompanied by an increase in scattering intensity, indicating an increase in phase separation. As would be expected for this series, a gradual increase in average interdomain spacing was observed as segment length increased.

The presence of an increasing number of single MDI units linking PHMO segments significantly reduces the electron density contrast between hard and soft domains, so much so in the case of H433 that no scattering occurs. Inclusion of more BDO in the system and longer segments introduces more incompatibility between hard and soft segments, and produces hard segments more capable of aggregation and crystallization.

Physical Testing

Tensile properties for this series of polyurethanes are given in Table VI, and typical tensile curves for the eight materials are shown in Figure 8. The initial slopes and stress values at low strains (~ 50%) show a stiffening of the materials as block length and degree of phase separation increase. H433 is below its T_g at room temperature, and also includes a significant amount of "fringed micelle" crystallinity, and is, therefore, the stiffest of all of the materials.

The polymers that have soft segments of molecular weights between 476 and 851 generally produce steep tensile curves in the region above 150% strain, and the slope of these curve sections decreases slightly for increasing block length. This is due to a higher concentration of urethane linkages in the soft domains of the "shorter block" materials, which in turn, enables stronger secondary bonding to take place during the stress crystallization process (the relatively poor tensile properties of H793 are possibly due to its lower molecular weight) (Table VII).

The tensile curves for H998 and H1180 indicate that very little stress crystallisation takes place in these materials and that the rigid networks present (possibly involving spherulites) impart high shear stresses at the domain interface causing permanent deformation and lower elongation values.

Shore-A hardness values increased for an increase in block length (apart from H433). The shore-D values also showed a general increase; however, the na-

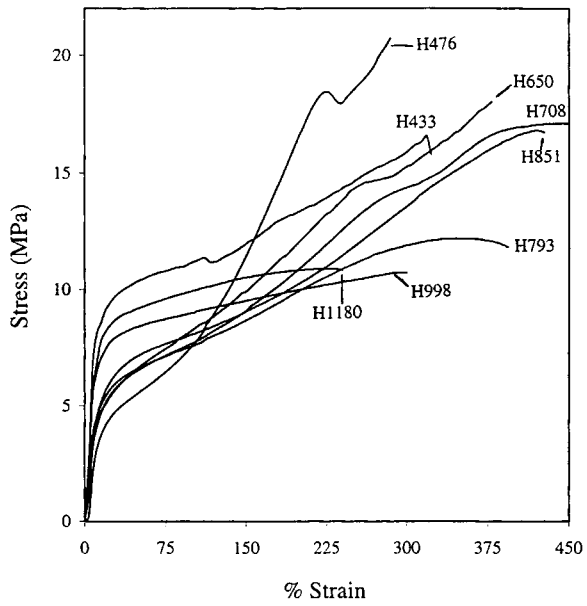

Figure 8 Typical tensile curves for the eight materials.

Table VI Tensile Properties

Material	UTS (MPa)	Fail Strain (%)	Permanent Set (%)	Stress at 100% Strain (MPa)
H433	17	348	27	11
H476	22	327	38	8
H650	17	462	61	8
H708	17	479	71	8
H793	12	416	78	8
H851	17	478	85	8
H998	11	384	99	9
H1180	11	255	67	10

Values displayed represent an average of five tests.

ture of this particular hardness test, which employs a sharper indentor at higher loads, means that the tear-resistance of the sample also has a bearing on the results. This phenomena may explain the lack of similar hardness rankings shown for the two indentors. Table VII also shows a general increase in molecular weight in the polyurethane series as segment length decreases. This is because the shorter segments are more mobile and compatible during the reaction/mixing procedure yielding a greater number of successful reactions.

CONCLUSIONS

The following conclusions have been drawn from this study:

increasing the segment length caused an increase in phase separation, average interdomain spacing, hardness, stiffness, and opacity. This was evidenced by a decrease in the soft microphase T_g, and an increase in the hard segment melting temperature(s), the degree of crystallinity, and the SAXS intensity of polymers in the series.

Four DSC melting endotherms of interest were encountered in the series and these were labeled T1, T2, T3, and T4. The results provided enough evidence to hypothesize that these four endotherms were a result of the disordering of structures including predominantly single MDI (whole chain, fringed micelle crystallinity), MDI_2BDO, MDI_3BDO_2, and MDI_4BDO_3 hard segments, respectively. It was also proposed that the sometimes broad T2 endotherm may be associated with the disordering of folded, longer hard segments.

For this system and composition ratio, optimum tensile properties (UTS and breaking strain) were achieved when a PHMO molecular weight of between 650 and 850 was employed. Longer soft segments provided soft domains that were partly paracrystalline. These soft domains also did not include as many hydrogen-bondable urethane linkages and, hence, were not as capable of forming effective stress crystallisable regions. This translated into a loss of the characteristic upturn in the stress–strain curves for H998 and H1180.

Table VII Molecular Weight and Hardness Values

Material	*Mn*/1000	Shore Hardness at 22°C	
		Shore A	Shore D
H433	98	88	47
H476	101	70	33
H650	89	80	38
H708	93	81	40
H793	53	81	37
H851	85	85	42
H998	63	89	41
H1180	61	90	41

The authors wish to acknowledge the assistance and helpful discussions contributed by Professor John White and Mr. Trevor Dowling regarding the SAXS results, and the help with thermal analysis provided by Mrs. M. Gertner. This work was supported by the CRC for Cardiac Technology and an Australian Postgraduate Research Award.

REFERENCES

1. R. Bonart and E. H. Muller, *J. Macromol. Sci. Phys.*, **B10,** 345 (1974).
2. C. P. Christenson et al., *J. Polym. Sci., Polym. Phys. Ed.*, **24,** 1401 (1985).
3. Y. Li, Z. Ren, M. Zhao, H. Yang, and B. Chu, *Macromolecules*, **26,** 612 (1993).

4.D. J. Martin, G. F. Meijs, G. M. Renwick, P. A. Gunatillake, and S. J. McCarthy, *J. Appl. Polym. Sci.*, to appear.
5.S. Abouzahr, G. L. Wilkes, and Z. Ophir, *Polymer*, **23**, 1077 (1982).
6. D. S. Huh and S. L. Cooper, *Polym. Eng. Sci.*, **11**, 369 (1971).
7. M. E. Kazmierczak, R. E. Fornes, D. R. Buchanan, and R. D. Gilbert, *J. Polym. Sci., Polym. Phys. Ed.*, **27**, 2188 (1989).
8. J. T. Koberstein, A. F. Galambos, and L. M. Leung, *Macromolecules*, **25**, 6195 (1992).
9. L. M. Leung and J. T. Koberstein, *J. Polym. Sci., Polym. Phys. Ed.*, **23**, 1883 (1985).
10. Z. S. Petrovic and I. Javni, *J. Polym. Sci., Polym. Phys. Ed.*, **27**, 545 (1989).
11. R. W. Seymour and S. L. Cooper, *Polym. Lett.*, **9**, 695 (1971).
12. J. W. C. Van Bogart, P. E. Gibson, and S. L. Cooper, *J. Polym. Sci., Polym. Phys. Ed.*, **21**, 65 (1983).
13. K. B. Wagener, *Macromolecules*, **25**, 5591 (1992).
14. R. S. Benson and D. J. Lyman, *J. Polym. Sci., Polym. Chem. Ed.*, **26**, 1393 (1988).
15. W. Chen, K. C. Frisch, D. J. Kenney, and S. Wong, *J.M.S.-Pure Appl. Chem.*, **A29**, 567 (1992).
16. B. Chu, T. Gao, Y. Li, J. Wang, C. R. Desper, and C. A. Byrne, *Macromolecules*, **25**, 5724 (1992).
17. Y. Chun, K. Kim, and J. Shin, *Polym. Int.*, **27**, 177 (1992).
18. L. L. Harrell, Jr., *Macromolecules*, **2**, 607 (1969).
19. T. R. Hesketh, J. W. C. Van Bogart, and S. L. Cooper, *Polym. Eng. Sci*, **20**, 190 (1980).
20. J. A. Miller, S. B. Lin, K. K. S. Hwang, K. S. Wu, P. E. Gibson, and S. L. Cooper, *Macromolecules*, **18**, 32 (1985).
21. H. N. Ng, A. E. Allegrezza, R. W. Seymour, and S. L. Cooper, *Polymer*, **14**, 255 (1973).
22. J. Blackwell and C. D. Lee, *J. Polym. Sci., Polym. Phys. Ed.*, **22**, 759 (1984).
23. W. Chen, *J. Polym. Sci., Polym. Phys.*, **29**, 1513 (1991).
24. R. F. Harris, M. D. Joseph, C. Davidson, C. D. Deporter, and V. A. Dais, *J. Appl. Polym. Sci.*, **41m** 509 (1990).
25. W. Hu and J. T. Koberstein, *J. Polym. Sci., Polym. Phys. Ed.*, **32**, 437 (1994).
26. J. T. Koberstein and A. F. Galambos, *Macromolecules*, **25**, 5618 (1992).
27. L. M. Leung and J. T. Koberstein, *Macromolecules*, **19**, 706 (1986).
28. Y. Li, T. Gao, and B. Chu, *Macromolecules*, **25**, 1737 (1992).
29. J. R. Quay, Z. Sun, J. Blackwell, R. M. Briber, and E. L. Thomas, *Polymer*, **31**, 1003 (1990).
30. T. P. Russel and J. T. Koberstein, *J. Polym. Sci., Polym. Phys. Ed.*, **23**, 1109 (1985).
31. A. J. Ryan, W. R. Willkomm, T. B. Bergstrom, C. W. Macosko, J. T. Koberstein, C. C. Yu, and T. P. Russel, *Macromolecules*, **24**, 2883 (1991).
32. S. L. Samuels and G. L. Wilkes, *J. Polym. Sci., Symp.*, **43**, 149 (1973).
33. J. W. C. Van Bogart, D. A. Bluemke, and S. L. Cooper, *Polymer*, **22**, 1428 (1981).
34. L. B. Liu, M. Sumita, K. Miyasaka, *Macromolecules*, **21**, 3424 (1988).
35. L. B. Liu, M. Sumita, K. Miyasaka, *J. Macromol. Sci. Phys.*, **B28**, 309 (1989).
36. M. Shibayama, T. Kawauchi, T. Kotani, S. Nomura, and T. Matsuda, *Polymer*, **18**, 719 (1986).
37. T. Yamamoto, M. Shibayama, S. S. Nomura, *Polym. Int.*, **21**, 895 (1989).
38. P. A. Gunatillake, G. F. Meijs, R. C. Chatelier, D. M. McIntosh, and E. Rizzardo, *Poylm. Int.*, **27**, 275 (1992).
39. *Annual Book of ASTM Standards*, (ASTM D2849-method C), 1975.
40. M. Aldissi, S. J. Henderson, J. W. White, and T. Zemb, *Mater. Sci. Forum*, **27/28**, 437 (1988).
41. P. A. Gunatillake et al., *J. Appl. Polym. Sci.*, **46**, 319 (1992).
42. G. F. Meijs, P. A. Gunatillake, E. Rizzardo, S. J. McCarthy, and R. C. Chatelier, in *Progress in Pacific Polymer Science 2*, Y. Imanishi, Ed., Springer Verlag, Berlin, 1992.
43. G. F. Meijs, S. J. McCarthy, E. Rizzardo, Y. Chen, R. C. Chatelier, A. Brandwood, and K. Schindhelm, *J. Biomed. Mater. Res.*, **27**, 345 (1993).
44. L. H. Peebles, Jr., *Macromolecules*, **7**, 872 (1974).
45. L. H. Peebles, Jr., *Macromolecules*, **9**, 58 (1976).
46. N. G. McCrum, B. E. Read, and G. Williams, *Anelastic and Dielectric Effects in Polymeric Solids*, Wiley, London, 1967.
47. D. J. Martin, PhD Thesis, University of Technology, Sydney, (CRC For Cardiac Technology) (1996).
48. J. Blackwell and C. D. Lee, *Structure and Morphology of the Hard Domains in Polyurethane Elastomers*, K. C. Frisch and D. Klempner, Eds., Advances in Urethane Science and Technology, Technomic, 1984.
49. R. Bonart, *J. Macromol. Sci. Phys.*, **B2**, 115 (1968).
50. L. Born, J. Chrone, H. Hespe, E. H. Muller, and K. H. Wolf, *J. Polym. Sci., Polym. Phys. Ed.*, **22**, 163 (1984).
51. K. K. S. Hwang, G. Wu, S. B. Lin, and S. L. Cooper, *J. Polym. Sci., Polym. Chem. Ed.*, **22**, 1677 (1984).
52. C. E. Wilkes and C. S. Yusek, *J. Macromol. Sci. Phys.*, **B7**, 157 (1973).

Received May 8, 1996
Accepted June 19, 1996